

REVISED DISTANCES TO 21 SUPERNOVA REMNANTS

S. RANASINGHE AND D.A. LEAHY¹

¹*Department of Physics & Astronomy, University of Calgary, Calgary, Alberta T2N 1N4, Canada*

(Received; Accepted; Published)

Submitted to ApJ

ABSTRACT

We carry out a comprehensive study of HI 21 cm line observations and ¹³CO line observations of 21 supernova remnants (SNRs). The aim of the study is to search for HI absorption features to obtain kinematic distances in a consistent manner. The 21 SNRs are in the region of sky covered by the Very Large Array Galactic Plane Survey (HI 21 cm observations) and Galactic Ring Survey (¹³CO line observations). We obtain revised distances for 10 SNRs based on new evidence in the HI and ¹³CO observations. We revise distances for the other 11 SNRs based on an updated rotation curve and new error analysis. The mean change in distance for the 21 SNRs is $\simeq 25\%$, i.e. change of 1.5 kpc compared to a mean distance for the sample of 6.4 kpc. This has a significant impact on interpretation of the physical state of these SNRs. For example, using a Sedov model, age and explosion energy scale as the square of distance, and inferred ISM density scales as distance.

Keywords: ISM: supernova remnants - radio continuum: ISM - radio lines: ISM

1. INTRODUCTION

Supernova remnants (SNRs) play an important role in determining the state of the interstellar medium of the Galaxy, as described in, e.g., the reviews by Cox (2005) and Ferrière (2001). However, in order to understand SNRs, reliable distances are necessary. Other objects, including HII regions and molecular clouds, are often associated with SNRs. To determine whether any given association is real, the SNR distance is needed.

One common method to find the distance to SNRs is to obtain kinematic distance from analysis of HI absorption spectra. This method has yielded reliable distance estimations, but it has been mainly applied to brighter SNRs. The HI absorption spectra of fainter SNRs are usually noisy. This is caused by real fluctuations, i.e. HI emission occurring at many random positions and velocities in both source and background regions used to create the absorption spectrum. For bright SNRs, these fluctuations are small compared to the absorption signal but for faint SNRs they are comparable. For the fluctuations in HI emission, the HI and continuum images are poorly correlated, whereas for real absorption there is a clear match between the absorption signal (decreased HI intensity) and the continuum emission. Thus careful investigation of the HI channel images is essential to assess the reality of any features which are seen in the HI absorption spectrum. Here we follow the analysis methods described by Leahy & Tian (2010) and Ranasinghe & Leahy (2017).

The sample of SNRs that we consider are those that cover the region of the VLA (Very Large Array) Galactic Plane Survey (VGPS) (Stil et al. 2006). There are 59 SNRs in the sky area covered by the VGPS survey. Of these, we have previously studied 10 SNRs without previous distance determinations, including SNRs G31.9+0.0 and G54.40.3 (Ranasinghe & Leahy 2017), 4 SNRs with new molecular cloud associ-

ations (Ranasinghe & Leahy 2017), and 4 SNRs without molecular cloud associations (Ranasinghe et al. 2017). In this work we analyze data for SNRs with previously published distances and for which the HI line data quality is high enough for analysis. This results in 21 SNRs in our sample presented here. For 10 of these SNRs, we revise previous distances based on new evidence from the HI and ^{13}CO data. For the remaining 11 SNRs, we confirm published kinematic velocities and revise distances using an updated error analysis and a more recent Galactic rotation curve. In Section 2, we present a brief description of the data, construction of HI absorption spectra and kinematic distances. The details for each of the 10 SNRs with new evidence are given in Section 3. The discussion and the final table summarizing our work for all 21 SNRs is described in Section 4.

2. DATA AND ANALYSIS

The HI line data and ^{13}CO line data are from the VGPS Survey (Stil et al. 2006) and the Galactic Ring Survey of the Five College Radio Astronomical Observatory (FCRAO) (Jackson et al. 2006). The method for making spectra and following analysis is from Leahy & Tian (2010) and Ranasinghe & Leahy (2017).

For kinematic distances, a reliable rotation curve is necessary. We adopt the universal rotation curve (URC) of Persic et al. (1996) with the Reid et al. (2014) parameters: Galactocentric radius of $R_0 = 8.34 \pm 0.16$ kpc and orbital velocity of the sun $V_0 = 241 \pm 8$ km s $^{-1}$. We verified the tangent point velocities predicted by this rotation curve as follows. For each SNR we obtained the HI emission spectrum adjacent to the SNR. We fit the high velocity part of the HI emission spectrum by a model spectrum of Galactic HI emission. The model spectrum was constructed by integrating, along the line of sight, the HI density as a function of position and velocity. The velocity of HI includes circular rotation and local Gaussian velocity dis-

persion. The adjustable parameters of interest from the fit were the circular velocity at the tangent point (thus tangent point velocity) and the velocity dispersion. The tangent point velocity obtained from the fit to the data agreed with that from the URC model within 3 km s^{-1} , except for 2 SNRs. For those 2 cases, the model fit and the URC tangent point velocities differ from significantly (see sections 3.9 and 3.10). The tangent point velocities from the fit to the data should be more reliable than from the URC, because the URC assumes an axisymmetric Galaxy, whereas the fit to the data does not. Thus the data fit allows for non-axisymmetric effects such as velocity perturbations due to spiral arms or the Galactic bar. We chose to use the tangent point velocities from the fits to the HI emission spectrum for those two cases.

To determine the tangent point error we use the error in $V_r = 5.3 \text{ km s}^{-1}$ (Ranasinghe & Leahy 2017). For the errors in the distances other than the tangent point, we follow the method presented by Ranasinghe & Leahy (2017).

3. RESULTS

For 10 of the 21 SNRs we obtain new evidence leading to different distances than previously published values. These SNRs are: G20.0–0.2, G23.6+0.3, G27.4+0.0, G33.6+0.1, G34.7–0.4, G39.2–0.3, G43.3–0.2, G46.8–0.3, G49.2–0.7 and G54.1 + 0.3. A brief overview of previous work and the arguments and relevant data for the new distances for each of these 10 SNRs are presented in the following sections. For the 11 SNRs for which we verify velocities from previous work, our results are presented only in the final table of distances. The distances for these 11 SNRs are different than previously published distances because we use an updated rotation curve.

3.1. G20.0 – 0.2

G20.0–0.2 was classified as a Crab-like supernova remnant (Becker & Helfand 1985). This was based on the flat radio spectral index, filled-center morphology and the presence of substantial polarization at 6 cm. To the north-left of the SNR, lies a compact and bright source, identified as the ultra-compact HII region GAL 20.08 – 0.14 (Wood & Churchwell 1989). Anderson et al. (2009) declared there is no ambiguity in position or velocity of this HII region. The velocity of 42.5 km s^{-1} yields the far side distance of 12.6 kpc (Petriella et al. (2013), Anderson & Bania (2009)).

Petriella et al. (2013) presented the first X-ray study, using archival Chandra observations to establish whether G20.0 – 0.2 is purely pleionitic or composite. They discovered diffuse X-ray emission with a non-thermal spectrum toward the center of the radio emission, so it is more likely the former. Using the ^{13}CO ($J = 1-0$) data of Jackson et al. (2006), Petriella et al. (2013) presented evidence of a molecular cloud extending from 62 to 72 km s^{-1} associated with the SNR. Using the velocity of 66 km s^{-1} the cloud is quoted to be at 4.5 or 11.5 kpc, and their analysis of the HI absorption favored the near distance.

Figure 1 shows the continuum image with region 1, chosen for HI absorption spectrum extraction. The HII region GAL 20.08–0.14 spectrum (Region 2) was used as a comparison. The HI spectra of the SNR and the HII region both show absorption present up to the tangent point (Figure 2). The spectrum of the SNR has a number of false features. These can be identified as caused by HI clouds in the source or background regions seen in the channel maps. For example, the 51.30 km s^{-1} image (Figure 3 left panel) shows a cloud in the source region (box 1) which results in $e^{-\tau} > 1$. Conversely a false absorption feature could be seen if the

higher intensity HI lies in the background region.

The absorption up to the tangent point is confirmed by the HI channel maps (Figure 3 right panel). Studying both spectra and the HI channels of the SNR, it is seen that there is clear absorption from ~ 110 km s $^{-1}$ to the tangent point velocity of ~ 123 km s $^{-1}$. The absorption features in the channel maps correlate morphologically to the brightest regions of the SNR and are highly likely to be real. Thus the lower limit distance to the SNR is the tangent point distance of 7.8 kpc.

From the ^{13}CO channel maps, the molecular clouds associated with the SNR are evident between 61.10 and 71.51 km s $^{-1}$ (see Petriella et al. (2013) Figure 5). Adopting 66.40 km s $^{-1}$ as the central velocity of the molecular cloud associated with the SNR, the distance to G20.00.4 is estimated to be 11.2 kpc.

The molecular cloud associated with the HII region GAL 20.08 – 0.14, is consistent with Anderson et al. (2009) analysis and has velocity of 42.5 km s $^{-1}$, yielding a distance of 12.4 kpc. The HII region is not associated with the SNR.

3.2. G23.6 + 0.3

SNR G23.6+0.3, is a $4' \times 10'$ object located in a complex region, in the close proximity to HII regions (e.g. WC89 (G023.71 + 00.17)). With a spectral index of 0.34 (Shaver & Goss 1970), the oddly elongated shape of the SNR coincides with $24 \mu\text{m}$ emission with no maser association (Pinheiro Gonçalves et al. 2011). Shaver & Goss (1970) quoted a distance of 6.4 kpc to the SNR. The survey Kilpatrick et al. (2016) for broad molecular line regions interacting with molecular clouds places it at a distance of 6.9 kpc.

The regions for extraction of HI absorption spectra are shown in Figure 4. Regions 1 and 2 were chosen to contain the brightest regions (~ 30 K) of the SNR and Region 3 was chosen for the HII region G023.71 + 00.17. The resulting spectra are shown in Figure 5. The spectra

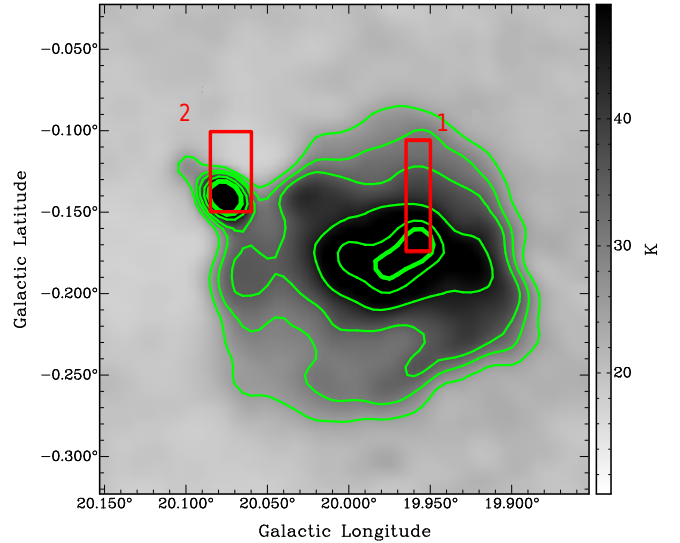


Figure 1. SNR G20.0 – 0.2 1420 MHz continuum image. Contour levels (green): 25, 30, 35, 45, 55 and 60 K. The red boxes are the regions used to extract HI and ^{13}CO source and background spectra.

of the SNR appear to show absorption up to the tangent point (~ 118 km s $^{-1}$). However the HI channel maps show that this absorption feature is false: the morphology of the brightest continuum regions do not correlate with the low HI intensity. Real absorption is seen is at a maximum radial velocity of 99.95 km s $^{-1}$ (Figure 6), consistent with the spectra and channel maps. The ^{13}CO channel maps show no clear evidence of a molecular cloud interaction. Therefore, we place the SNR at the near distance of 5.9 kpc that corresponds to the radial velocity of 99.95 km s $^{-1}$.

The nearby HII region G23.710 + 0.175 shows absorption up to the tangent point indicating lower limit of distance of 7.6 kpc. Jones & Dickey (2012) presents the radio recombination line velocity of 103.8 km s $^{-1}$ and a distance of $7.78^{+1.03}_{-1.19}$ kpc. Using the URC rotation curve we find the distance to the HII region for that velocity to be 9.2 kpc.

3.3. G27.4 + 0.0

Known as 4C-04.71 and Kes 73, SNR G27.4 + 0.0 is a shell-type SNR, $4.5' \times 5'$ in size. It is lo-

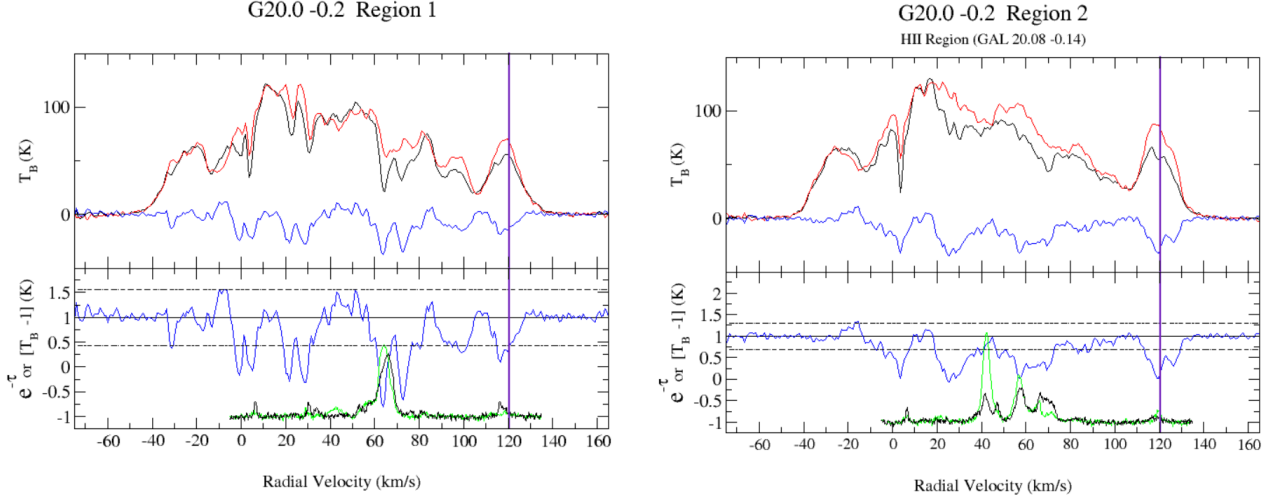


Figure 2. SNR G20.0 – 0.2 (left) and HII region GAL 20.08 – 0.14 (right) spectra. Upper half of panel: HI emission spectrum (source: black, background: red and difference: blue). Lower half of panel: HI absorption spectrum ($e^{-\tau}$, blue), ^{13}CO source (green) & background (black) spectra (T_B , offset by subtracting 1 K), $\pm 2\sigma$ noise level of the HI absorption spectrum (dashed line) and tangent point velocity (purple vertical line).

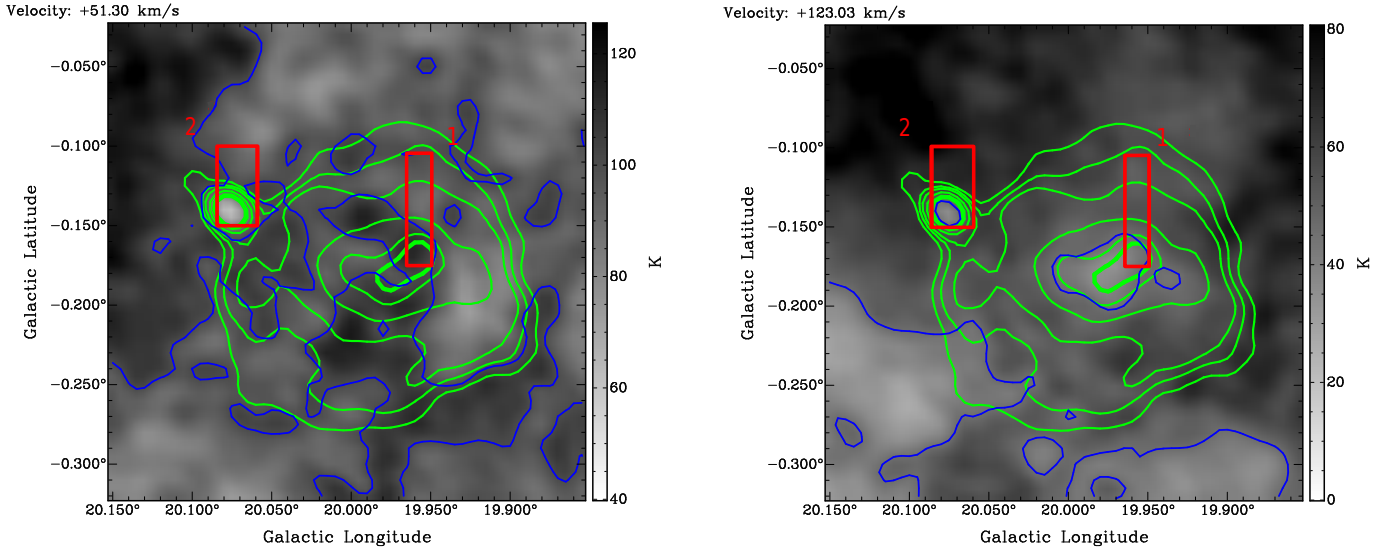


Figure 3. G20.0 – 0.2 HI channel maps $+51.30$ and $+123.03$ km s^{-1} . HI contour levels (blue): 46 and 100 K respectively. Continuum contour levels (green): 25, 30, 35, 45, 55 and 60 K.

cated near two HII regions, G27.276+0.148 and G27.491 + 0.189. From the X-ray spectrum of the SNR, [Gotthelf & Vasisht \(1997\)](#) give the age to be ≤ 2.2 kyr. The compact central source, 1E 1841-045 associated with G27.4+0.0 was discovered by [Vasisht et al. \(2000\)](#) as an Anomalous X-ray pulsar (AXP). They interpreted its ~ 11.8 s pulse period and high spin-down rate to obtain a characteristic age of 4.7 kyr.

[Sanbonmatsu & Helfand \(1992\)](#) presented HI absorption observations for the SNR with estimated distance 6 - 7.5 kpc. [Tian & Leahy \(2008\)](#) revised the distance to be 7.5- 9.8 kpc, leading to an updated age for the SNR of 500-1000 yr and a larger AXP X-ray luminosity.

We constructed HI absorption spectra and verified the absorption features examining the HI channel maps. The spectra are essentially

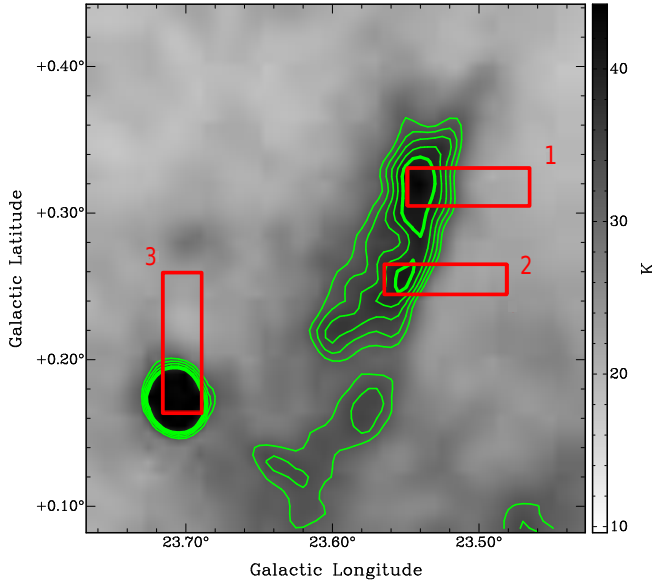


Figure 4. SNR G23.6 + 0.3 1420 MHz continuum image. Contour levels (green): 32, 34, 36, 38 and 40 K. The red boxes are the regions used to extract HI and ^{13}CO source and background spectra.

the same as given in Figure 2 of Tian & Leahy (2008). Even though the spectra show absorption features up to the tangent point, the channel maps show that the morphology of HI absorption does not match the continuum intensity of the SNR. Thus the absorption near the tangent point is most likely a false feature. The maximum radial velocity where HI absorption for the SNR is seen in the channel maps is 99.95 km s^{-1} (Figure 7 top panel). The conclusion that the SNR is located at the near distance of 5.8 kpc.

We see there is clear absorption for the nearby HII regions up to the tangent point not seen in the SNR (Figure 7 bottom panel). Thus the SNR and the nearby HII regions are not related.

3.4. G33.6 + 0.1

G33.6 + 0.1, is a shell-type SNR located in a complex region. Also known as Kes 79, 4C00.70, HC13 and G33.7 + 0.0, the SNR is $\sim 10'$ in size and has a bright central region (Figure 8). Giacani et al. (2009) noted the SNR is likely the product of the gravitational collapse of a O9 star

evolving near a molecular cloud and within a wind-driven bubble. The compact X-ray source CXOU J185238.6 + 0.004020 is located close to the geometric center of the SNR and has no association with a radio point source or pulsar wind nebula. Caswell et al. (1975) presented an HI absorption spectrum for positive velocities and, because HI absorption was seen up to the tangent point, suggested a lower limit distance of 7 kpc. Frail & Clifton (1989), scaling the dispersion measure distance with the ratio of the optical depth integrals, estimated a distance of $10 \pm 2 \text{ kpc}$ for the SNR. Kilpatrick et al. (2016) confirmed a broad line detection and presented a distance of 7.1 kpc consistent with the HI absorption.

Three spectra extracted from the bright regions (boxes in Figure 8) are shown in Figure 9). The left arc and the center, both are bright with a $T_B \sim 50 - 70 \text{ K}$. The three spectra show several inconsistent features which can be attributed to random clouds that can be seen in the HI channel maps. The spectra shows no consistent HI absorption at negative velocities. This was verified using the individual HI channel maps. HI absorption is consistently present in all regions in the spectra and HI channel maps at a velocity of 57.90 km s^{-1} (Figure 10 top panel). There is no evidence of HI absorption up to the tangent point at $\sim 108 \text{ km s}^{-1}$ (Figure 10 bottom panel), even though clear absorption is seen in the nearby objects. From this we derive the distance to the SNR is 3.5 kpc.

The examination of ^{13}CO channel maps show molecular clouds in the vicinity. These molecular clouds do not morphologically correlate with G33.6 + 0.1. The most likely scenario is that these molecular clouds are behind the SNR.

3.5. G34.7 - 0.4

The SNR G34.7 - 0.4 is $\sim 35' \times 27'$ in size. It is also known as W44, G34.6 - 0.5 and 3C392. It is a relatively bright remnant with an elongated and distorted shell lying in a complex region,

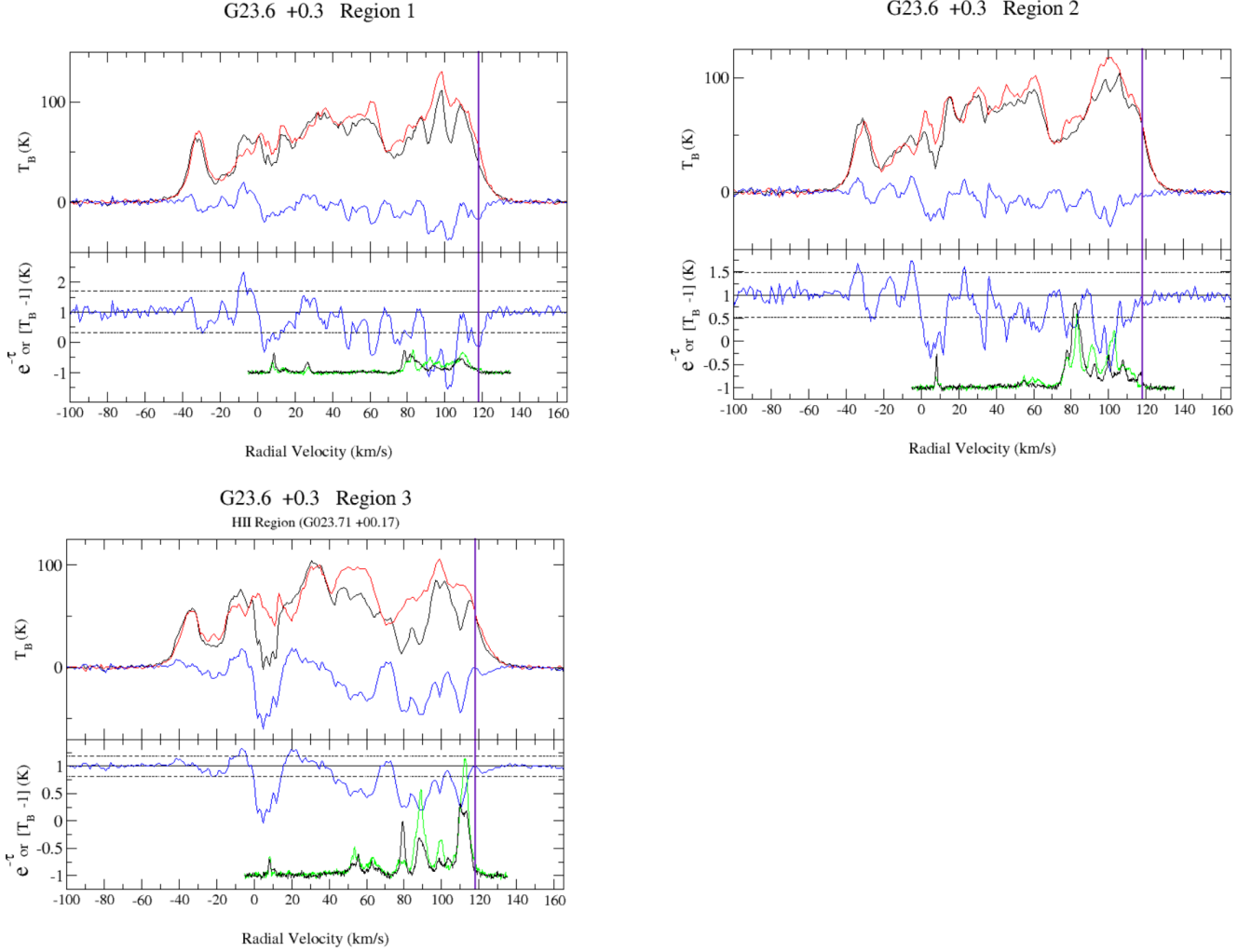


Figure 5. G23.6 + 0.3 spectra (top and middle) and HII region G023.71 + 00.17 (bottom) spectrum. Upper half of panel: HI emission spectrum (source: black, background: red and difference: blue). Lower half of panel: HI absorption spectrum ($e^{-\tau}$, blue), ^{13}CO source (green) & background (black) spectra (T_B , offset by subtracting 1 K), $\pm 2\sigma$ noise level of the HI absorption spectrum (dashed line) and tangent point velocity (purple vertical line).

in close proximity to several molecular clouds. Radhakrishnan et al. (1972) found the distance to be 3 kpc using HI absorption spectra. This estimate is consistent with OH emission and H_2CO absorption profiles showing strong features at $+45 \pm 5 \text{ km s}^{-1}$ (Ilovaisky & Lequeux 1972). Caswell et al. (1975) found the same distance but with improved HI absorption spectra. Cox et al. (1999) revised the distance estimate to 2.5 - 2.6 kpc using a different Galactic rotation curve and $R_0 = 8.5 \text{ kpc}$.

Figure 11 shows the regions chosen for extrac-

tion of HI absorption spectra. The western arc of the SNR is the brightest, and all regions were of brightness temperature $T_B > 120 \text{ K}$ for the source region. All the spectra are consistent with each other, showing no absorption at negative velocities. Therefore, we present only the region 4 spectrum (Figure 12). There is no absorption seen up to the tangent point, indicating the SNR is at the near kinematic distance. Continuous strong absorption is seen in the velocity range $0 - \sim 50 \text{ km s}^{-1}$. The HI channel map at $V_r = 50.48 \text{ km s}^{-1}$ confirms the absorption

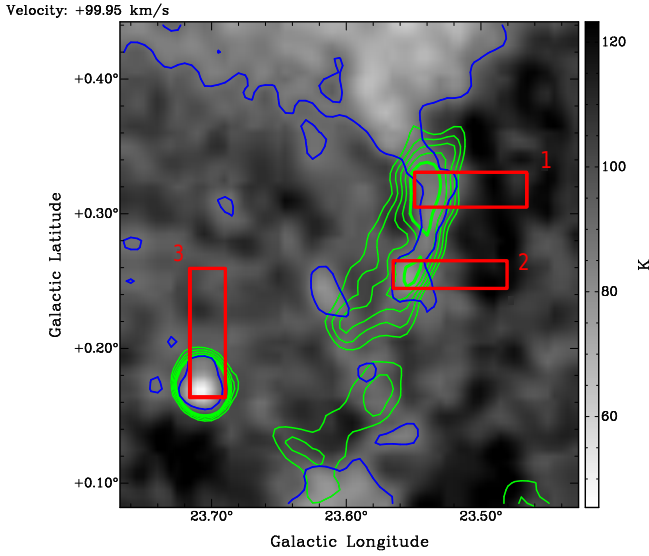


Figure 6. G23.6 + 0.3 HI channel map +99.95 km s⁻¹. HI contour level (Blue): 90 K . Continuum contour levels (green): 32, 34, 36, 38 and 40 K.

along the southern border (Figure 13), yielding a distance of 3.0 kpc.

The ¹³CO channel maps yield no strong evidence of molecular cloud interactions. There is no morphological evidence that the molecular cloud seen at the velocity range ~ 42 to ~ 50 km s⁻¹ is interacting with the SNR.

3.6. G39.2 – 0.3

Also known as 3C396, HC24 and NRAO 593, the SNR G39.2 – 0.3 is $\sim 8' \times 7'$ in size. The radio shell is brighter to the right with a faint tail to the left of the SNR. The western shell that is bright in radio and X-ray emission is suggestive of molecular cloud interaction (Hewitt et al. 2009). The SNR is located near the HII region NRAO 591. Caswell et al. (1975) reported HI absorption present up to the tangent point (7.7 kpc). Furthermore, they stated that because the absorption is almost continuous from 60 km s⁻¹, the lower limit is 11.3 kpc. Green (1984) pointed out that the feature at the tangent point of Caswell et al. (1975) may be false and suggested the tangent point distance of 7.7 kpc as the only lower limit distance to the SNR. Later, they revised the lower limit distance to the

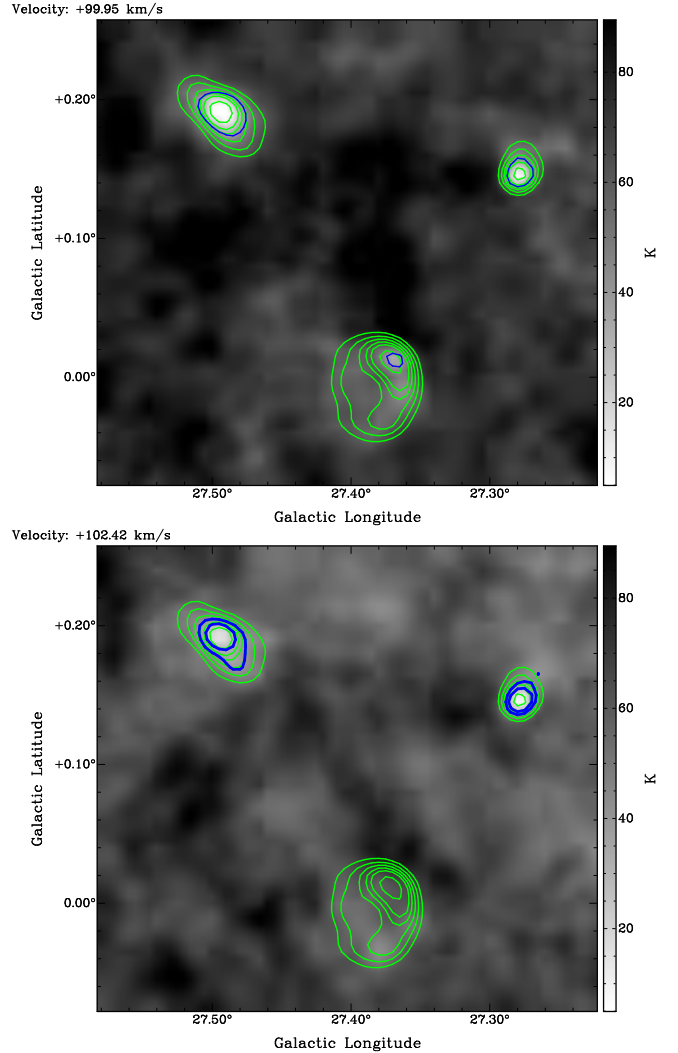


Figure 7. G27.4 + 0.0 HI channel maps +99.95 and +102.42 km s⁻¹. HI contour level (Blue): 40 K for HI channel map +99.95 km s⁻¹ and 30 & 40 K for HI channel map 102.42 km s⁻¹. Continuum contour levels (green): 35, 40, 50, 60, 70, 80 and 100 K.

SNR was 6.6 kpc Green (1989). Based on HI self-absorption, Su et al. (2011) placed the SNR at a distance of 6.2 kpc (tangent point).

Using the Σ -D relation, Patnaik et al. (1990) estimated the distance and diameter 7.3 kpc and 16.5 pc respectively for the SNR and 14 kpc for the HII region NRAO 591. The Σ -D relation is an observed correlation for SNR with known distances between radio surface brightness Σ and physical diameter D . Generally,

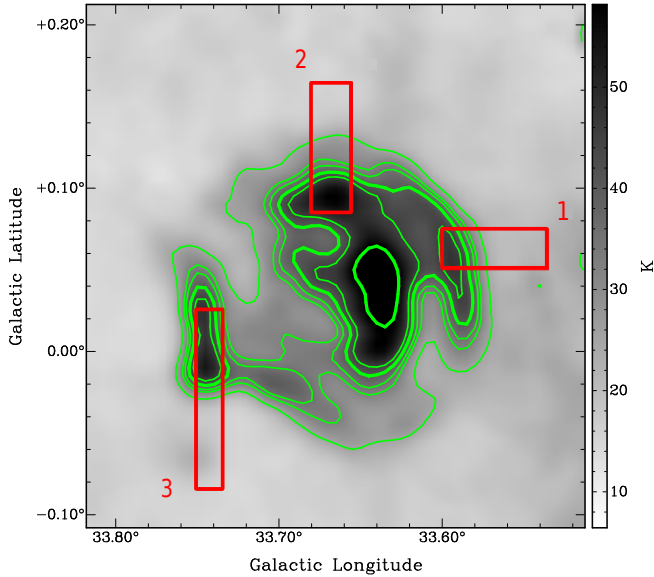


Figure 8. SNR G33.6 + 0.1 1420 MHz continuum image. Contour levels (green): 25, 32, 35, 40, 45 and 60 K. The red boxes are the regions used to extract HI and ^{13}CO source and background spectra.

larger SNRs have lower surface brightness. It has quite large scatter (Green 2015), severely limiting its usefulness.

We constructed the spectrum for the SNR using the northern bright region ($T_B = \sim 120$) and found it to be the same as in Su et al. (2011) (their Figure 7). HI absorption is present up to the tangent point yielding a lower limit to the distance of 6.4 kpc.

The ^{13}CO channel maps indicate a cavity-like structure between the velocities 67.69 and 70.88 km s^{-1} (Figure 14 top panel). This structure was seen by Su et al. (2011) and is consistent with ^{12}CO observations. They suggest the cloud seen at $\sim 84 \text{ km s}^{-1}$ is more likely to be associated with the SNR. From the ^{13}CO channel maps, between the velocities 83.63 – 85.12 km s^{-1} there is a possible molecular cloud interaction (Figure 14 bottom panel). However the cavity-like structure at $\sim 69 \text{ km s}^{-1}$ spatially correlates better with the SNR. Therefore we take the likely distance to G39.2 – 0.3 as 8.5 kpc corresponding to the velocity of 69.4 km s^{-1} .

3.7. G43.3 – 0.2

Known as W49B, the relatively young SNR G43.3 – 0.2 is located in the W49 complex which includes one of the most luminous star forming regions in our galaxy. The object W49A (G43.2 – 0.0) near the SNR consists of numerous HII regions (Brogan & Troland 2001). Early analyses have stated the two objects that are separated by $\sim 12'$ are physically associated with each other. Analysis of HI absorption carried out by Lockhart & Goss (1978) gave the lower and upper limits of distance to G43.3 – 0.2 as 12.5 kpc and 14 kpc. They noted that the SNR and HII region W49A are possibly associated with each other. Moffett & Reynolds (1994) revised the distances to 8 and 11 kpc, respectively. Gwinn et al. (1992) estimated the distance to W49A to be 11.4 ± 1.2 kpc from H_2O maser proper motions.

Figure 15 shows the continuum image with regions used for spectrum extraction. All three spectra are consistent so we present the Region 1 spectrum in Figure 16. Absorption is seen up to the tangent point. This is verified in the HI channel map (Figure 17 top panel). The lower limit of the distance to the SNR is the tangent point distance of 6.0 kpc. Examination of the HI channels at negative velocities shows there is no absorption so the SNR is inside the Solar circle. The SNR spectrum shows absorption throughout the positive velocities, except with no absorption at velocity $\sim 12 \text{ km s}^{-1}$. The HI channel map shows absorption in the HII region but not in the SNR (Figure 17 bottom panel). This shows that the SNR is most likely located just this side of $V_r \simeq 12.55 \text{ km s}^{-1}$, corresponding to a distance of 11.3 kpc.

The HII region W49A shows absorption up to the tangent point. However, W49A shows strong absorption at negative velocities, up to $V_r = -22.07 \text{ km s}^{-1}$, beyond the Solar circle at a corresponding distance of 13.7 kpc. Radhakrishnan et al. (1972) places the HII region

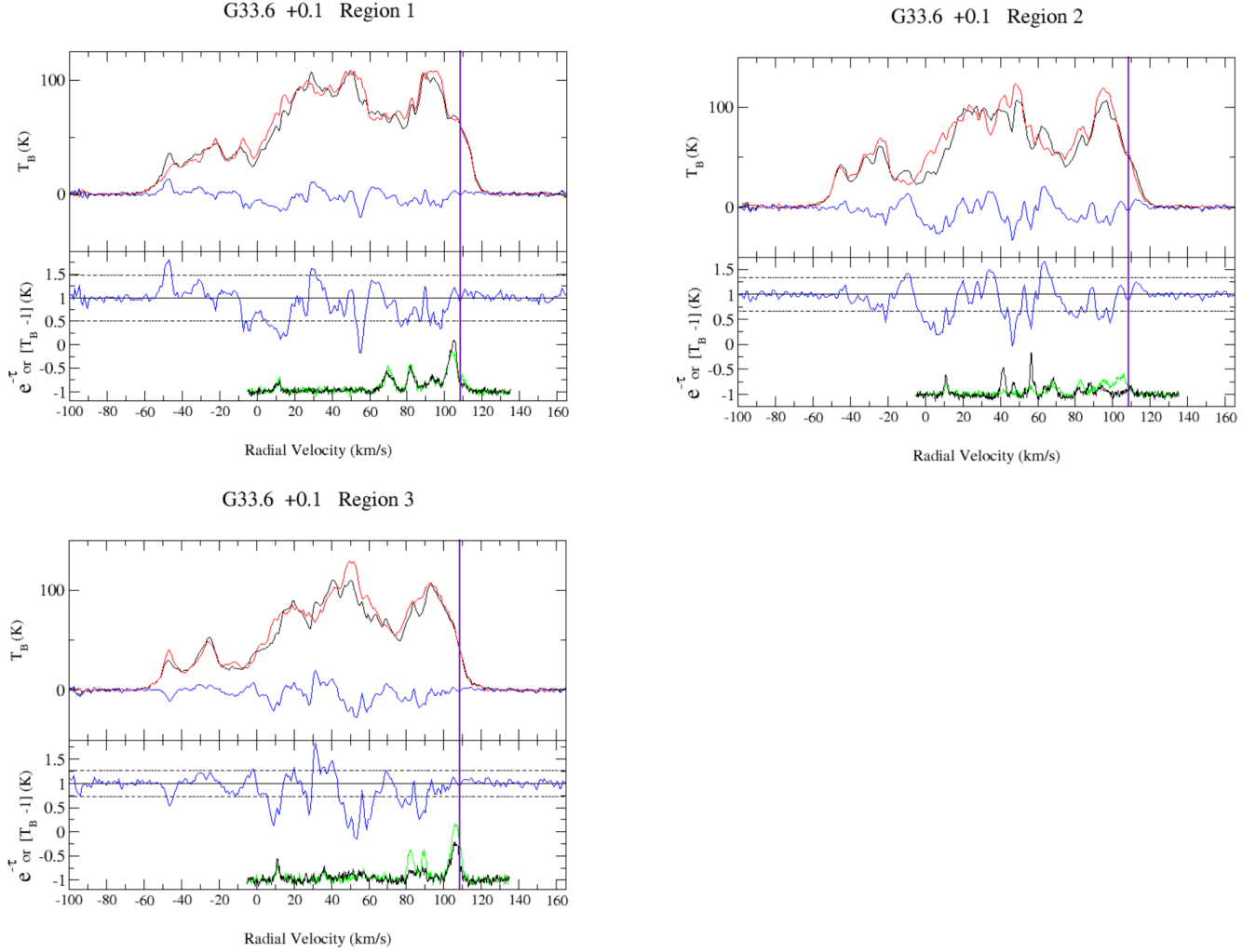


Figure 9. G33.6 + 0.1 spectra. Upper half of panel: HI emission spectrum (source: black, background: red and difference: blue). Lower half of panel: HI absorption spectrum ($e^{-\tau}$, blue), ^{13}CO source (green) & background (black) spectra (T_B , offset by subtracting 1 K), $\pm 2\sigma$ noise level of the HI absorption spectrum (dashed line) and tangent point velocity (purple vertical line).

at ~ 14 kpc which is consistent with the absorption velocity and distance derived in this study. The distance to the HII region W49A, of 13.7 kpc makes it highly unlikely that it's associated with the SNR.

Comparison of the ^{13}CO emission and HI absorption spectra shows that prominent molecular clouds have corresponding HI absorption. Individual ^{13}CO channel maps show no evidence of molecular clouds associated or interacting with G43.3 – 0.2.

3.8. G46.8 – 0.3

The $16' \times 17'$ SNR G46.8 – 0.3 (HC30) is located near the HII region G46.2 – 0.2 (Figure 18). It has an almost complete shell with bright arcs to the north-west and south-east. Based on 1.7 and 2.7 GHz observations, Willis (1973) first identified the SNR. Sato (1979) suggested a distance between 6.8 and 8.6 kpc from HI absorption and emission features.

The region 4 spectrum is shown in Figure 19. HI absorption occurs up to the tangent point velocity at $\sim 65 \text{ km s}^{-1}$, thus the SNR is located beyond the tangent point distance of 5.7 kpc. There are no absorption features at nega-

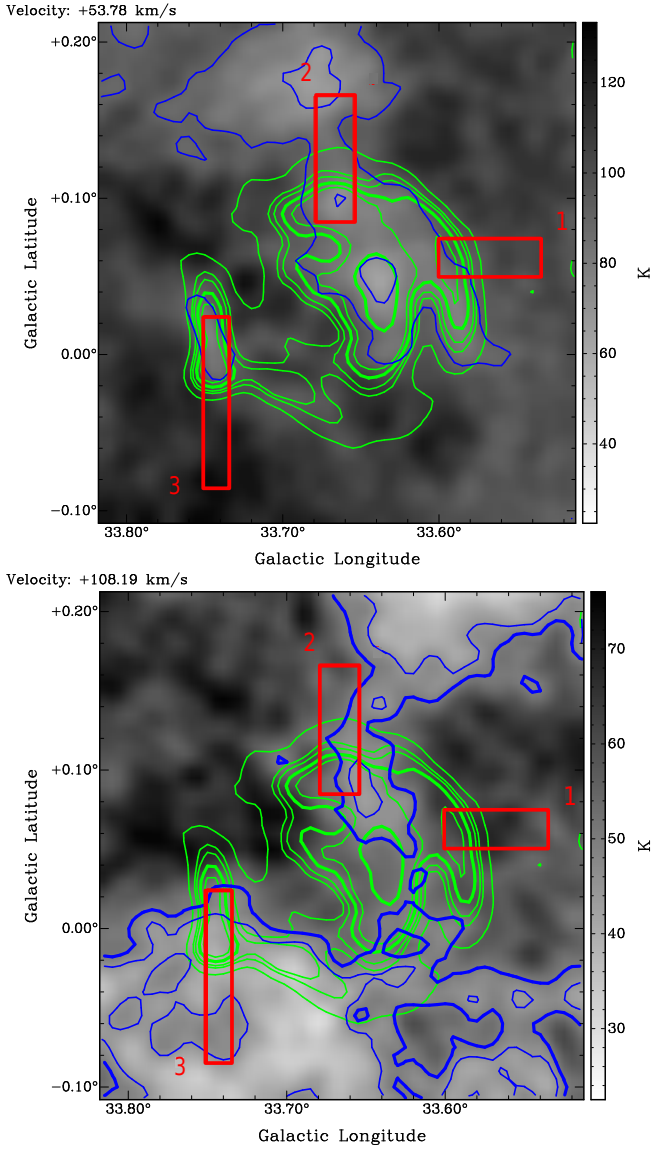


Figure 10. G33.6 + 0.1 HI channel maps +53.78 and +108.19 km s^{-1} . HI contour levels (Blue): 45 and 50 K. Continuum contour levels (green): 25, 32, 35, 40, 45 and 60 K.

tive velocities giving the upper limit distance at the far side of the solar circle (11.4 kpc).

Quireza et al. (2006) places the HII region at a distance of 7.8 kpc beyond the tangent point. The HI channel maps show that the HI absorption for the HII region does not extend to the tangent point (64 km s^{-1}) and the maximum velocity where the absorption is seen is at $\sim 57 \text{ km s}^{-1}$. This velocity is consistent with the radio recombination line velocity (RRL) of 57.09

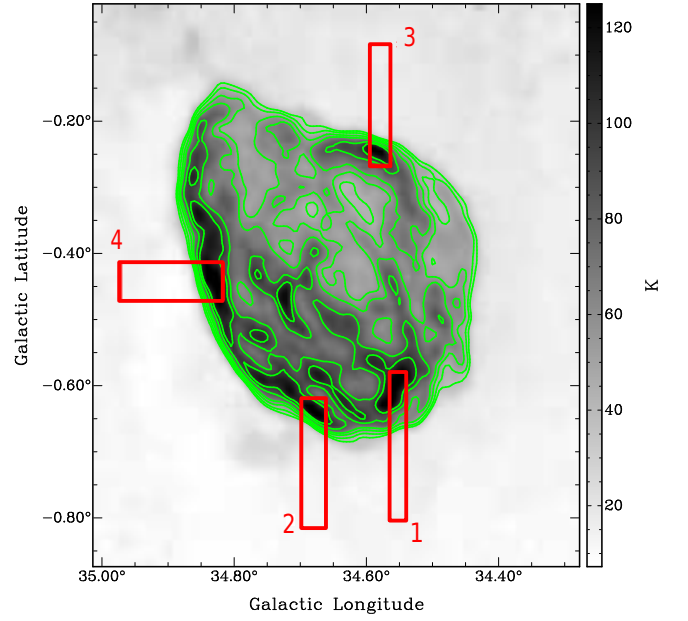


Figure 11. SNR G34.7 – 0.4 1420 MHz continuum image. Contour levels (green): 38, 45, 55, 65, 85 and 100 K. The red boxes are the regions used to extract HI and ^{13}CO source and background spectra.

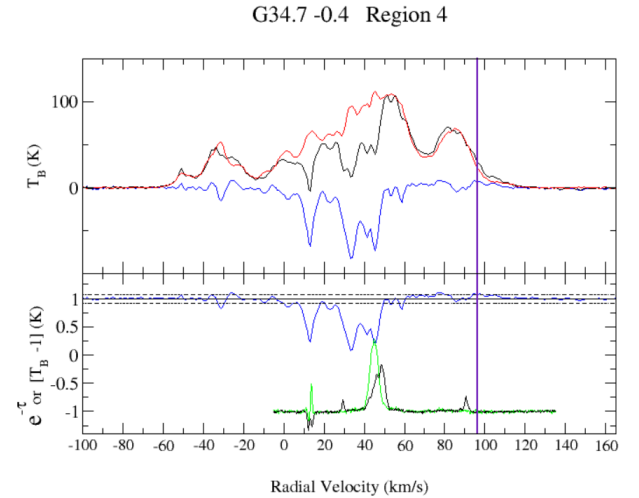


Figure 12. G34.7 – 0.4 spectrum. Upper half of panel: HI emission spectrum (source: black, background: red and difference: blue). Lower half of panel: HI absorption spectrum ($e^{-\tau}$, blue), ^{13}CO source (green) & background (black) spectra (T_B , offset by subtracting 1 K), $\pm 2\sigma$ noise level of the HI absorption spectrum (dashed line) and tangent point velocity (purple vertical line).

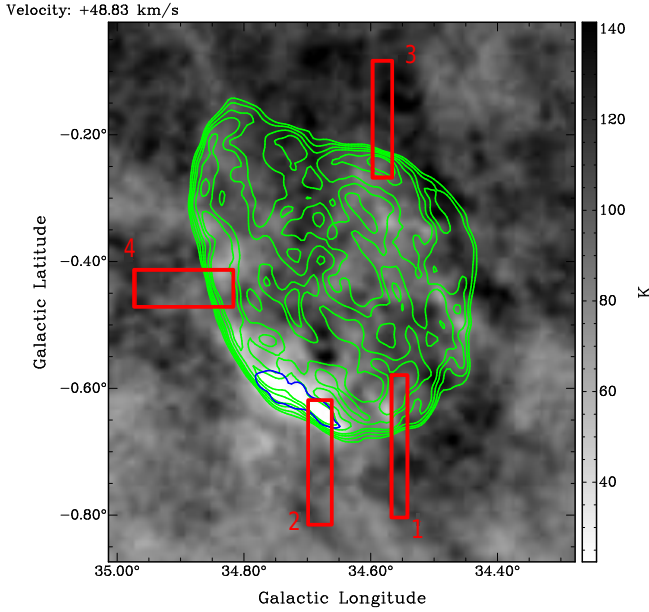


Figure 13. G34.7 – 0.4 HI channel map +48.83 km s⁻¹. HI contour level (Blue): 30 K. Continuum contour levels (green): 38, 45, 55, 65, 85 and 100 K.

km s⁻¹ (Quireza et al. 2006). We place the HII region at the near-distance of 4.1 kpc.

3.9. G49.2 – 0.7

Known as W51C, G49.2 – 0.7 is located in the W51 complex, a star forming complex that consist of HII regions W51A, W51B and the SNR W51C (Tian & Leahy (2013) Figure 1). The SNR is a partial shell that extends on to the complex W51B. Magnetohydrodynamic simulations were carried out to disentangle the SNR from its surrounding emission (Zhang et al. 2017). Sato (1973) used HI absorption to estimate the distance of W51C as 4.1 kpc. Koo et al. (1995) associated G49.2 – 0.7 with a high-velocity molecular cloud that placed the SNR at ~6 kpc, near the the tangent point distance, but points out the cloud may extend over 1.5 kpc along the line of sight making it unclear where the SNR is located. Tian & Leahy (2013) reported a distance of 4.3 kpc to the SNR using HI absorption spectra.

Our HI absorption spectra are essentially the same as given in Figure 2 of Tian & Leahy

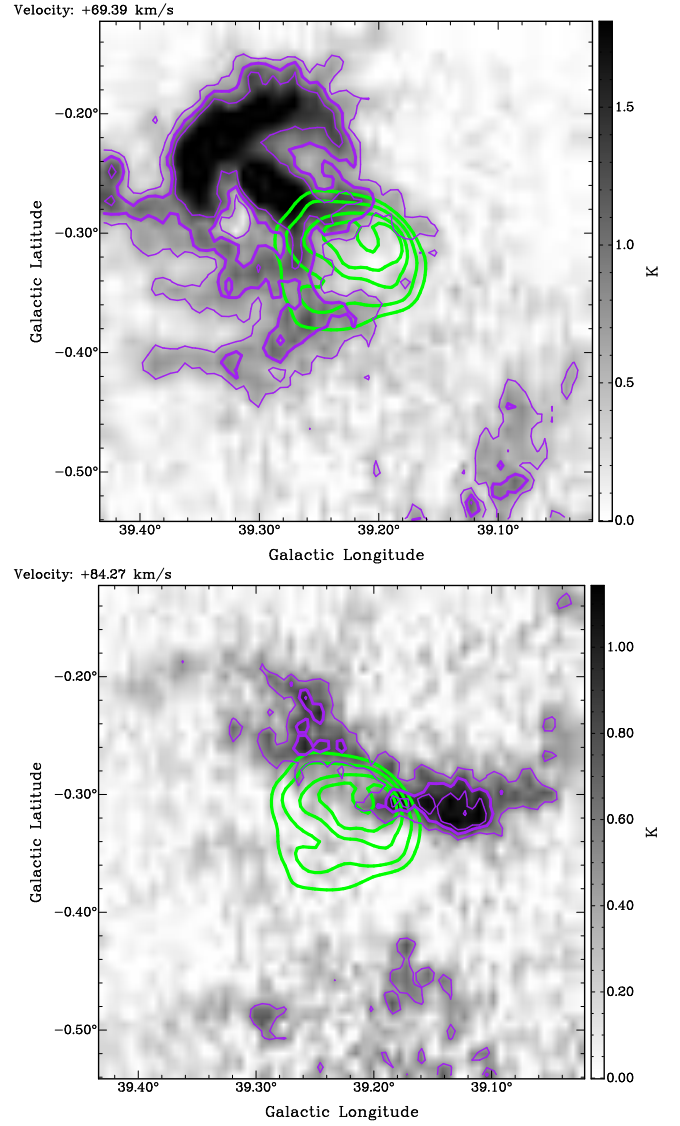


Figure 14. G39.2–0.3 ¹³CO channel maps +69.39 and +84.27 km s⁻¹. ¹³CO contour levels (purple): 0.5, 0.8 and 1.2 K for +69.39 km s⁻¹ channel map and 0.5, 0.8 and 1.0 K +84.27 km s⁻¹. Continuum contour levels (green) are at 30, 50, 80 and 100 K.

(2013). The rotation curve (URC with Reid et al. (2014) parameters) yields a tangent point velocity of 57.8 km s⁻¹, inconsistent with the emission spectrum towards the SNR. Our fit of the observed HI profile including a Gaussian velocity dispersion yields a tangent point velocity of 65.6 km s⁻¹. Absorption is present up to the tangent point, giving a lower limit distance to the SNR of the tangent point dis-

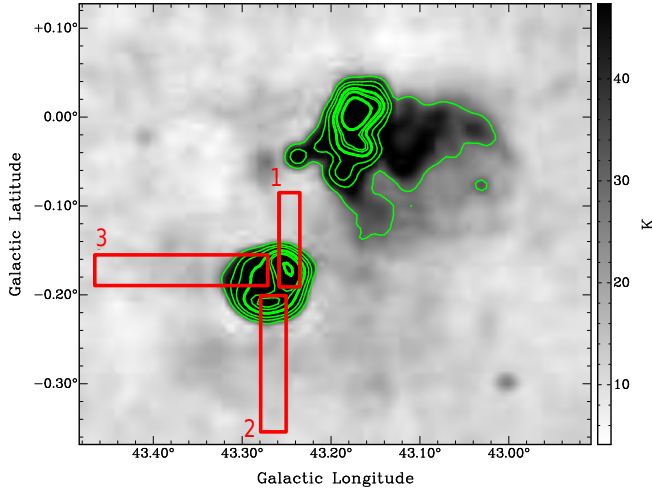


Figure 15. SNR G43.3 – 0.2 1420 MHz continuum image. Contour levels (green): 30, 60, 100, 200, 300, 350, 500 and 600 K. The red boxes are the regions used to extract HI and ^{13}CO source and background spectra.

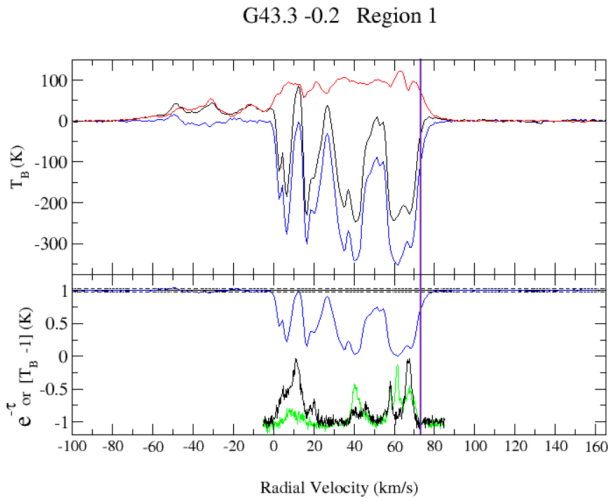


Figure 16. G43.3 – 0.2 spectrum. Upper half of panel: HI emission spectrum (source: black, background: red and difference: blue). Lower half of panel: HI absorption spectrum ($e^{-\tau}$, blue), ^{13}CO source (green) & background (black) spectra (T_B , offset by subtracting 1 K), $\pm 2\sigma$ noise level of the HI absorption spectrum (dashed line) and tangent point velocity (purple vertical line).

tance 5.4 kpc. [Koo & Moon \(1997\)](#) noted the molecular cloud associated with the SNR is at $62 \pm 2 \text{ km s}^{-1}$. The nearby HII regions ([Quireza](#)

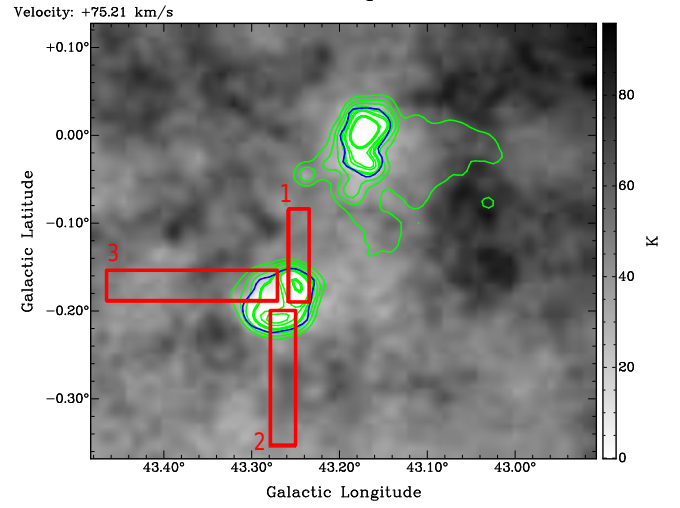
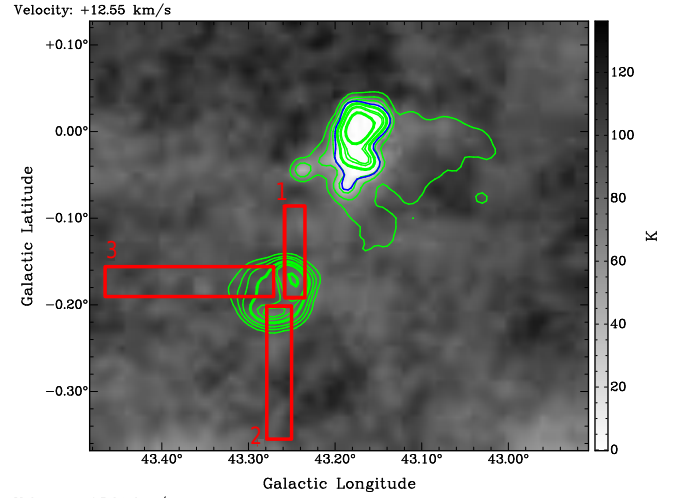


Figure 17. G43.3 – 0.2 HI channel maps at 75.21 and 12.55 and km s^{-1} . HI contour levels (Blue): 20 K. Continuum contour levels (green): 30, 60, 100, 200, 300, 350, 500 and 600 K.

[et al. 2006](#)) G48.930 – 0.28, G48.997 – 0.29, G49.204 – 0.34 and G49.384 – 0.30 have RRL velocities of 65.86, 66.86, 67.79 and 67.38 km s^{-1} respectively. [Quireza et al. \(2006\)](#) places the HII regions at $\sim 5.6 \text{ kpc}$ (tangent point with $R_0 = 8.5 \text{ kpc}$). We conclude that the SNR and the HII regions are likely associated with each other and place the SNR and the HII regions at a distance of 5.4 kpc.

3.10. G54.1 + 0.3

The $\sim 12'$ SNR is a possible composite type remnant around the Crab-like pulsar wind nebula (PWN) G54.1 + 0.3 and located near the

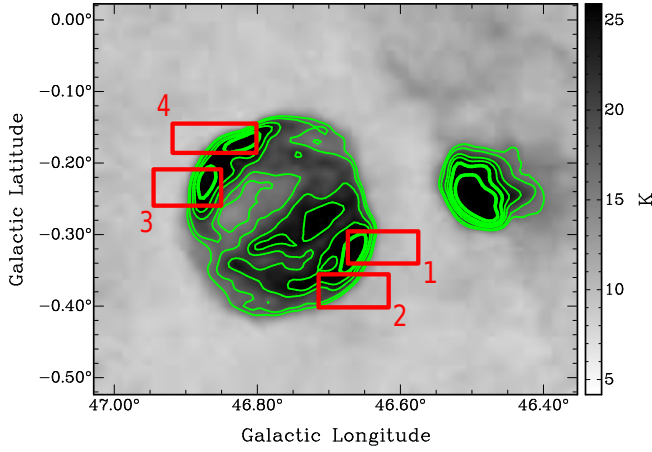


Figure 18. SNR G46.8 – 0.3 1420 MHz continuum image. Contour levels (green) at 16, 18, 22, 25, 30 and 40 K. The red boxes are the regions used to extract HI and ^{13}CO source and background spectra.

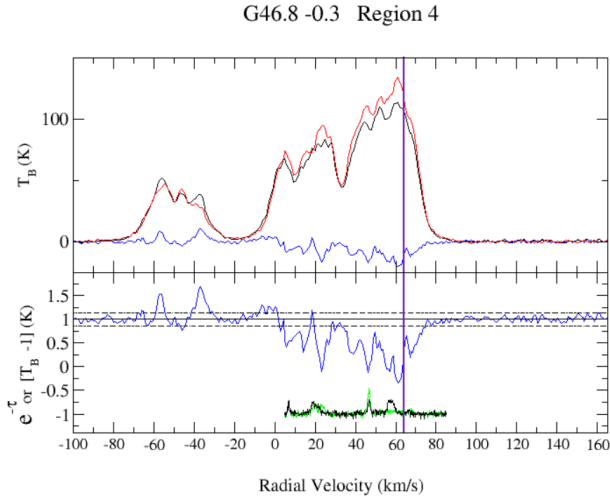


Figure 19. G46.8 – 0.3 spectrum. Upper half of panel: HI emission spectrum (source: black, background: red and difference: blue). Lower half of panel: HI absorption spectrum ($e^{-\tau}$, blue), ^{13}CO source (green) & background (black) spectra (T_B , offset by subtracting 1 K), $\pm 2\sigma$ noise level of the HI absorption spectrum (dashed line) and tangent point velocity (purple vertical line).

HII region G54.09 – 0.06, and compact sources G53.83 – 0.06 and G54.1 + 0.1 (Leahy et al. 2008). The relatively bright pulsar wind nebula core is $\sim 3'$ across. Lu et al. (2002) estimated the distance to the SNR as ~ 5 kpc, based on X-

ray observations, with absorption column density about half the Galactic absorption. Leahy et al. (2008) gave a distance of 4.5 – 9 kpc to the SNR, using HI absorption spectra. They suggested the morphological association of the PWN with a molecular cloud at 53 km s^{-1} yields the likely distance to the SNR of $6.2_{-0.6}^{+1.0}$ kpc.

Our HI spectra for the PWN are the same as Figure 2 in Leahy et al. (2008). The URC rotation curve gives a tangent point velocity of 45.5 km s^{-1} , inconsistent with the emission spectrum towards the SNR. Our fit of the observed HI profile including a Gaussian velocity dispersion yields a tangent point velocity of 52.8 km s^{-1} , very different than that assumed by Leahy et al. (2008). The associated ^{13}CO molecular cloud at 53.66 km s^{-1} (Leahy et al. (2008) Figure 3) places the SNR at the tangent point. Therefore, the distance to the SNR is 4.9 kpc.

4. DISCUSSION AND SUMMARY

We have analyzed HI 21 cm line observations and ^{13}CO line observations of 21 supernova remnants (SNRs) which are located in the sky area of the VGPS survey. The Galactic rotation curve we use for that area of the Galaxy is the URC rotation curve with Reid et al. (2014) parameters. We examined 1420 MHz continuum emission, HI emission and absorption spectra, ^{13}CO emission spectra and the HI line ^{13}CO line channel maps. We obtain new observational evidence for 10 SNRs and thus revise their distances to be different than previously published values. For the other 11 SNRs, we confirm the kinematic velocities but use an updated error analysis and the updated rotation curve to revise distances. The uncertainties in V_r and the resulting distance are discussed in Ranasinghe & Leahy (2017).

Table 1 presents our results for the 21 SNRs. The literature distances are presented with a note on the method, whether by HI absorption, association with molecular cloud or by the $\Sigma - D$ relation. The various assumed values of radial

velocity for the SNR and parameters of the rotation curve (R_0 and V_0) used in previous distances are listed in columns 4 to 6. Our current most likely radial velocity, V_r is listed in column 8. Column 9 notes whether the SNR is at the near side or far side of the tangent point, or at the tangent point. The new distance is listed in column 10. Column 11 notes whether there is an association of the SNR with a molecular cloud.

We note that previous work has used a wide range of Galactic rotation curves, usually assuming $V(R)$ is constant. In some cases the assumed rotation curve is not quoted. The mean and standard deviation for the quoted R_0 values is 8.25 kpc and 0.56 kpc, and for the $V - 0$ values is 223 km s⁻¹ and 12 km s⁻¹. This range in R_0 and V_0 can by itself lead to a range of distances. For many cases our radial velocities are similar to those in the literature. They agree within 5 km s⁻¹ for 9 cases, are very different for 3 cases, and for the remaining cases there is no well defined value in the literature.

Next we discuss the improvement to the distances to the SNRs, in addition to the fact that we use a consistent rotation curve here, rather than the different rotation curves used for each SNR in the literature.

The distance has significantly changed (more than 2σ), based on our consistently derived errors, for 9 SNRs G18.1 - 0.1, G18.8 + 0.3, G20.0 - 0.2, G23.3 - 0.3, G23.6 + 0.3, G27.4 + 0.0, G33.6 + 0.1, G39.2 - 0.3 and G54.1 + 0.3. For 8 SNRs the old and new distances agree within 2σ : SNRs G18.6 - 0.2, G21.5 - 0.9, G22.7 - 0.2, G32.8 - 0.1, G34.7 - 0.4, G35.6 - 0.4, G41.1 - 0.3 and G46.8 - 0.3. For 4 SNRs the previous distance was very poorly known G21.8 - 0.6, G29.7 - 0.3, G43.3 - 0.2 and G49.2 - 0.7. Including the first two groups of 21 SNRs, the mean change in distance is 1.5 kpc. This is quite significant, considering the distance range is 3 to 13.8 kpc with mean 6.4 kpc. I.e. on average

the distance improvement is 23.4%. The largest change in distance is for G20.2 - 0.2 which went from an old estimate of 4.5 kpc to a new value of 11.2 kpc. The improved distances have a significant effect on the physical interpretation of supernova remnants. For example, we use the Sedov model equations as given in Cox (1972). The inferred shock radius R_s of an SNR depends linearly on distance, d . As described in Leahy & Williams (2017), the ISM density n_0 depends on the emission measure, EM , as \sqrt{EM} , and EM depends on distance as d^2 . Explosion energy E_0 depends on EM , thus on d^2 . For the Sedov model, the important quantity is E_0/n_0 , which depends linearly on distance. SNR age in the Sedov model depends on $R_s^{5/2}(n_0/E_0)^{1/2}$, thus depends on d^2 . For more sophisticated models, the scaling with distances are not as simple as this, but the change in results is similar.

In summary, we have obtained distances to a significant number of SNRs using a consistent method and rotation curve. Follow-up work will investigate the implications for the ages and evolutionary states of these SNRs by incorporating other data. For example, with X-ray spectra the shock temperature and the emission measure can be determined. These can be used to estimate physical properties of SNRs using explosion models. Easy-to-use SNR explosion models can be based on analytical fits to numerical explosion calculations. Such models have been presented by Leahy & Williams (2017), based on the Truelove & McKee (1999) models. These models have been applied to the set of LMC SNRS by Leahy (2017) to obtain important properties of the SNR population, including finding a log-normal distribution of explosion energies, the LMC SNR birthrate, and the distribution of ISM densities around SNRs in the LMC. Similar methods will be applied to learn about the properties of Galactic SNRs.

ACKNOWLEDGEMENTS

Table 1. Distances to supernova remnants

#	Source	Literature					New results			$^{13}\text{CO}^c$
		Dist ^a (kpc)	V_r (km s ⁻¹)	R_0 (kpc)	V_0 (km s ⁻¹)	Refs	V_r (km s ⁻¹)	KDAR ^b	Dist (kpc)	
01	G18.1 -0.1	5.6 ^H	100	8.5	210	1	103.74	N	6.4 ± 0.2	Possible
02	G18.6 -0.2	4.6 ± 0.6 ^H	62	8.5	220	2	62.84	N	4.4 ± 0.2	No
03	G18.8 +0.3	12.1 ^{HM}	20	7.6	214	3	21.35	F	13.8 ± 0.4	Yes
04	G20.0 -0.2	4.5 ^M	66	8.5	220	4	66.40	F	11.2 ± 0.3	Yes
05	G21.5 -0.9	4.7 ± 0.4 ^H	68	8	220	5	67.79	N	4.4 ± 0.2	No
06	G21.8 -0.6	5.5 ^{HM}	86	8.0	220	6A	93.35	N	5.6 ± 0.2	Yes
		5.2 ^{HM}	85	8.0	220	6B				
07	G22.7 -0.2	4.4 ± 0.4 ^M	77	8.31	241	7	76.63	N	4.7 ± 0.2	Yes
08	G23.3 -0.3	3.9 – 4.5 ^{HM}	66 - 80	7.6	214	8	78.51	N	4.8 ± 0.2	Yes
09	G23.6 +0.3	6.9 ^{M S}	9	99.95	N	5.9 ± 0.2	Possible
10	G27.4 +0.0	7.5 – 9.8 ^H	$V_{TP} - 84$	8.5	220	10	99.95	N	5.8 ± 0.3	No
11	G29.7 -0.3	5.1 – 7.5 ^{HM}	95 - 102	7.6	220	11A	95.00	N	5.6 ± 0.3	Yes
		10.6 ^M	54	8.0	220	11B				
12	G32.8 -0.1	4.8 ^{HM}	~ 81	8.0	220	12	81.81	N	4.8 ± 0.3	Yes
13	G33.6 +0.1	7.1 ^{MS}	9	57.90	N	3.5 ± 0.3	No
14	G34.7 -0.4	2.5 – 2.6 ^H	42	8.5	220	14	50.48	N	3.0 ± 0.3	No
15	G35.6 -0.4	3.6 ± 0.4 ^{HM}	~ 61	8.5	220	15	63.67	N	3.8 ± 0.3	Possible
16	G39.2 -0.3	6.2 ^{HM}	84	8.0	220	16	69.39	F	8.5 ± 0.5	Yes
17	G41.1 -0.3	8 – 9.7 ^H	...	8.33	218	17	$V_{TP} - 63.01$	F	8.5 ± 0.5	No
18	G43.3 -0.2	8 – 11 ^H	18	12.55	F	11.3 ± 0.4	No
19	G46.8 -0.3	6.8 – 8.6 ^H	$V_{TP} - 59$	10.0	250	19	$V_{TP} - 0$	TP – F	5.7 ± 0.9 – 11.4 ± 0.5	No
20	G49.2 -0.7	4.3 ^H	70.7	8.4	254	20A	V_{TP}	TP	5.4 ± 0.6	No
		6 ^M	V_{TP}	8.5	...	20B				
21	G54.1 +0.3	5.6 – 7.2 ^{HM}	53 ± 12	7.6	220	21	53.66	TP	4.9 ± 0.8	Yes

NOTE—

^aLiterature distance estimation method - Superscript H: HI absorption, M: Molecular cloud association/interaction and S: Σ -D relation.^bKDAR- Kinematic Distance Ambiguity Resolution, indicating whether the SNR is at the near (N), far (F) or tangent point (TP) distance.^cAssociated with ^{13}CO .

References— (1) Leahy et al. (2014), (2) Johanson & Kerton (2009), (3) Tian et al. (2007), (4) Petriella et al. (2013), (5) Tian & Leahy (2008), (6A) Tian & Leahy (2008), (6B) Zhou et al. (2009), (7) Su et al. (2014), (8) Leahy & Tian (2008), (9) Kilpatrick et al. (2016), (10) Tian & Leahy (2008), (11A) Leahy & Tian (2008), (11B) Su et al. (2009), (12) Zhou & Chen (2011), (14) Cox et al. (1999), (15) Zhu et al. (2013), (16) Su et al. (2011), (17) Leahy & Ranasinghe (2016), (18) Brogan & Troland (2001), (19) Sato (1979), (20A) Tian & Leahy (2013), (20B) Koo et al. (1995), (21) Leahy et al. (2008).

This work was supported in part by a grant from the Natural Sciences and Engineering Research Council of Canada.

REFERENCES

Anderson, L. D., & Bania, T. M. 2009, ApJ, 690, 706

Anderson, L. D., Bania, T. M., Jackson, J. M., et al. 2009, ApJS, 181, 255

- Becker, R. H., & Helfand, D. J. 1985, *ApJL*, 297, L25
- Brogan, C. L., & Troland, T. H. 2001, *ApJ*, 550, 799
- Caswell, J. L., Murray, J. D., Roger, R. S., Cole, D. J., & Cooke, D. J. 1975, *A&A*, 45, 239
- Cox, D. P. 1972, *ApJ*, 178, 159
- Cox, D. P., Shelton, R. L., Maciejewski, W., et al. 1999, *ApJ*, 524, 179
- Cox, D. P. 2005, *ARA&A*, 43, 337
- Ferrière, K. M. 2001, *Reviews of Modern Physics*, 73, 1031
- Frail, D. A., & Clifton, T. R. 1989, *ApJ*, 336, 854
- Giacani, E., Smith, M. J. S., Dubner, G., et al. 2009, *A&A*, 507, 841
- Gotthelf, E. V., & Vasisht, G. 1997, *ApJL*, 486, L133
- Green, D. A. 1984, *MNRAS*, 209, 449
- Green, D. A. 1989, *MNRAS*, 238, 737
- Green, D. A. 2014, *Bulletin of the Astronomical Society of India*, 42, 47
- Green, D. A. 2015, *MNRAS*, 454, 1517
- Green, D. A. 2017, *VizieR Online Data Catalog*, 7278
- Gwinn, C. R., Moran, J. M., & Reid, M. J. 1992, *ApJ*, 393, 149
- Hewitt, J. W., Rho, J., Andersen, M., & Reach, W. T. 2009, *ApJ*, 694, 1266
- Ilovaisky, S. A., & Lequeux, J. 1972, *A&A*, 18, 169
- Jackson, J. M., Rathborne, J. M., Shah, R. Y., et al. 2006, *ApJS*, 163, 145
- Johanson, A. K., & Kerton, C. R. 2009, *AJ*, 138, 1615
- Jones, C., & Dickey, J. M. 2012, *ApJ*, 753, 62
- Kilpatrick, C. D., Bieging, J. H., & Rieke, G. H. 2016, *ApJ*, 816, 1
- Koo, B.-C., & Moon, D.-S. 1997, *ApJ*, 475, 194
- Koo, B.-C., Kim, K.-T., & Seward, F. D. 1995, *ApJ*, 447, 211
- Kwee, K. K., Muller, C. A., & Westerhout, G. 1954, *BAN*, 12, 211
- Leahy, D. A., & Tian, W. W. 2008, *AJ*, 135, 167
- Leahy, D. A., & Tian, W. W. 2008, *A&A*, 480, L25
- Leahy, D., & Tian, W. 2010, *The Dynamic Interstellar Medium: A Celebration of the Canadian Galactic Plane Survey*, 438, 365
- Leahy, D. A., Tian, W., & Wang, Q. D. 2008, *AJ*, 136, 1477
- Leahy, D., Green, K., & Tian, W. 2014, *MNRAS*, 438, 1813
- Leahy, D. A., & Ransinghe, S. 2016, *ApJ*, 817, 74
- Leahy, D. A., & Williams, J. E. 2017, *AJ*, 153, 239
- Leahy, D. A. 2017, *ApJ*, 837, 36
- Lockhart, I. A., & Goss, W. M. 1978, *A&A*, 67, 355
- Lu, F. J., Wang, Q. D., Aschenbach, B., Durouchoux, P., & Song, L. M. 2002, *ApJL*, 568, L49
- Moffett, D. A., & Reynolds, S. P. 1994, *ApJ*, 437, 705
- Patnaik, A. R., Hunt, G. C., Salter, C. J., Shaver, P. A., & Velusamy, T. 1990, *A&A*, 232, 467
- Persic, M., Salucci, P., & Stel, F. 1996, *MNRAS*, 281, 27
- Petriella, A., Paron, S. A., & Giacani, E. B. 2013, *A&A*, 554, A73
- Pinheiro Gonçalves, D., Noriega-Crespo, A., Paladini, R., Martin, P. G., & Carey, S. J. 2011, *AJ*, 142, 47
- Quireza, C., Rood, R. T., Balser, D. S., & Bania, T. M. 2006, *ApJS*, 165, 338
- Quireza, C., Rood, R. T., Bania, T. M., Balser, D. S., & Maciel, W. J. 2006, *ApJ*, 653, 1226
- Radhakrishnan, V., Goss, W. M., Murray, J. D., & Brooks, J. W. 1972, *ApJS*, 24, 49
- Ransinghe, S., & Leahy, D. A. 2017, *ApJ*, 843, 119
- Ransinghe, S., & Leahy, D. A. 2017, [arXiv:1712.04423](https://arxiv.org/abs/1712.04423)
- Ransinghe, S., Leahy, D. A., & Tian, W. 2017, [arXiv:1712.04515](https://arxiv.org/abs/1712.04515)
- Reid, M. J., Menten, K. M., Brunthaler, A., et al. 2014, *ApJ*, 783, 130
- Sanbonmatsu, K. Y., & Helfand, D. J. 1992, *AJ*, 104, 2189
- Sato, F. 1973, *PASJ*, 25, 135
- Sato, F. 1979, *Astrophys. Lett.*, 20, 43
- Shaver, P. A., & Goss, W. M. 1970, *Australian Journal of Physics Astrophysical Supplement*, 14, 133
- Stil, J. M., Taylor, A. R., Dickey, J. M., et al. 2006, *AJ*, 132, 1158
- Su, Y., Chen, Y., Yang, J., et al. 2009, *ApJ*, 694, 376
- Su, Y., Chen, Y., Yang, J., et al. 2011, *ApJ*, 727, 43
- Su, Y., Yang, J., Zhou, X., Zhou, P., & Chen, Y. 2014, *ApJ*, 796, 122
- Tian, W. W., & Leahy, D. A. 2008, *MNRAS*, 391, L54

- Tian, W. W., & Leahy, D. A. 2008, *ApJ*, 677, 292-296
- Tian, W. W., & Leahy, D. A. 2013, *ApJL*, 769, L17
- Tian, W. W., Leahy, D. A., & Wang, Q. D. 2007, *A&A*, 474, 541
- Truelove, J. K., & McKee, C. F. 1999, *ApJS*, 120, 299
- Vasisht, G., Gotthelf, E. V., Torii, K., & Gaensler, B. M. 2000, *ApJL*, 542, L49
- Willis, A. G. 1973, *A&A*, 26, 237
- Wood, D. O. S., & Churchwell, E. 1989, *ApJS*, 69, 831
- Zhang, M. F., Tian, W. W., Leahy, D. A., et al. 2017, *ApJ*, 849, 147
- Zhou, P., & Chen, Y. 2011, *ApJ*, 743, 4
- Zhou, X., Chen, Y., Su, Y., & Yang, J. 2009, *ApJ*, 691, 516
- Zhu, H., Tian, W. W., Torres, D. F., Pedalletti, G., & Su, H. Q. 2013, *ApJ*, 775, 95